Dark Matter in Compact Objects (TBD)

Michael Virgato
0000-0002-8396-0896

Submitted in total fulfilment
of the requirements of the degree of

Doctor of Philosophy

School of Physics
The University of Melbourne

XXX XXX

Produced on archival quality paper.

Abstract

DM in COs Heat up Maybe See

Publications

Refs. [1–6] below are the journal publications, and preprints authored or co-authored during my PhD candidature. The authors are listed alphabetically in all of the titles.

Journal papers and preprints

[1] Papers

Declaration

This is to certify that

1. the thesis comprises only my original work towards the PhD except where indicated in the preface;
2. due acknowledgement has been made in the text to all other material used;
3. the thesis is less than 100,000 words in length, exclusive of tables, maps, bibliographies and appendices.

Michael Virgato, XXX XXX

Preface

We don't know what DM is. Can NSs constrain it?

Acknowledgements

Why did I do this?

Contents

List of Figures

List of Tables

1 Introduction

Dark Matter is an enigma in modern physics. Despite the significant scientific effort that has gone into trying to discern its nature, a definitive detection proving its existence eludes us. Nevertheless, dark matter's influence on our Universe is undeniable, with evidence supporting its existence arising on all scales, large and small.

1.1 Evidence for Dark Matter

Today, the amount of evidence in support of dark matter's existence is overwhelming. This evidence comes from astrophysical and cosmological observations inconsistent with a universe composed entirely of visible matter. This section serves as a review of this evidence.

1.1.1 Astrophysical Observations

Galaxy Clusters

Some of the first hints of dark matter's existence came from observations of galaxy clusters. Perhaps the most famous analysis was performed by Fritz Zwicky [7], who was puzzled by the high rotational velocities of galaxies within the Coma Cluster. By applying the virial theorem, equating the cluster's kinetic and gravitational potential energies, he found that the cluster would need to contain a much more significant amount of *dunkle materie* (dark matter) than visible matter to accommodate these high velocities.

Rotation Curves of Spiral Galaxies

The anomalous rotational velocities observed in galaxy clusters can also be observed at the galactic scale. The rotation curves of spiral galaxies, which relate the rotational velocities of stars to their distance from the galactic centre, were observed to be flat at large distances. From the observed distribution of visible matter, Newtonian mechanics predicts that the orbital velocity of a star a distance r from the galactic centre, $v_\star(r)$, is related to the mass of the galaxy, $M(r)$, through

$$v_\star(r) = \sqrt{\frac{GM(r)}{r}}, \tag{1.1}$$

indicating that the velocity should fall off as $1/\sqrt{r}$ at the outer regions of the galaxy where $M(r)$ is constant. Instead, observations of many spiral galaxies indicate that this velocity remains constant out to the galaxy's edge.

A simple way to produce such a rotation curve is to introduce a spherically symmetric distribution of dark matter around the galaxy,

$$\rho_{\mathrm{DM}}(r) = \frac{v_0^2}{4\pi G r^2}, \tag{1.2}$$

that results in a constant rotational velocity of v_0 out to the galaxy edge. Detailed simulations of structure formation in a Cold Dark Matter (CDM) Universe indicate that the dark matter halo follows a Navaro-Frenk-White (NFW) profile, **cite for NFW**

$$\rho_{\mathrm{DM}}(r) = \frac{\rho_0}{\left(\frac{r}{r_{\mathrm{s}}}\right)\left(1+\frac{r}{r_{\mathrm{s}}}\right)^2}, \tag{1.3}$$

where ρ_0 and r_{s} are free parameters that must be fit to each halo.

An example rotation curve for galaxy NGC 6503 is presented in Fig. 1.1, with the contributions from each of the matter components to the rotational velocity shown [8, 9]. As can be seen, the visible matter constituting disk and gas components does not explain the observed rotational velocity.

Gravitational Lensing

As General Relativity describes, the curvature of space-time around massive entities causes light to travel along curved paths. As such, the mass of astrophysical structures can be deduced from the extent to which objects in the background are gravitationally lensed. The disparity between the mass obtained from gravitational lensing and the mass of visible matter in the system is further evidence of dark matter's existence.

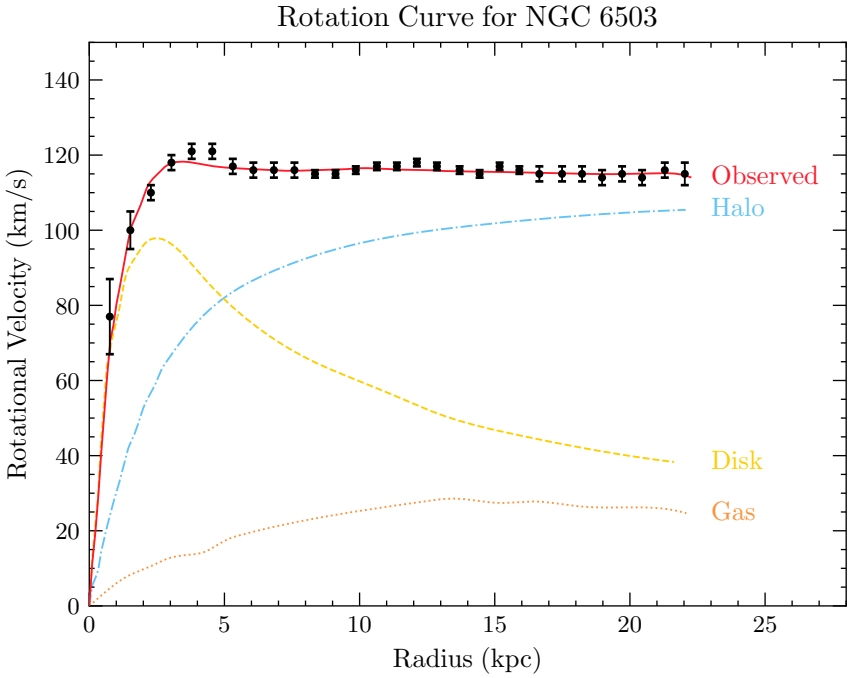

Figure 1.1: Galaxy rotation curve for NGC 6503, showing the contributions to the total velocity (red) from the DM halo (blue), disk (yellow), and gas components. Data used in making this plot was obtained from [8, 9].

The Bullet Cluster

The bullet cluster is the result of two colliding galaxy clusters which the Chandra X-ray telescope imaged. When viewed in the X-ray, the smearing of the visible matter after the collision is clearly seen, as shown in the red regions of Fig. 1.2, which is expected from such a collision. However, when the gravitational potential was mapped using gravitational lensing, it was clear that the majority of the mass was displaced relative to the visible matter. This mass is attributed to the dark matter components of the original clusters. As indicated by the purple regions in Fig. 1.2, the dark matter halos seem to have passed through each other mostly unperturbed. This tells us that not only is the majority of the mass comprised of dark matter, but that the dark matter has extremely small interactions with both the visible matter and itself.

1.1.2 Cosmological Evidence

Dark matter has played a major role in the cosmological history of our Universe. The current best cosmological model is the Λ-Cold Dark Matter model (ΛCDM), in

Figure 1.2: Image of the Bullet Cluster with contours of the gravitational potential superposed. The red regions indicate the baryonic matter after the collision, while the purple regions are the expected DM components deduced from gravitational lensing. cite

which cold (i.e. non-relativistic) dark matter plays a prominent role. The relative amount of dark matter present in our Universe can be determined with measurements of the light element abundances produced via Big Bang Nucleosynthesis (BBN).

The Cosmic Microwave Background

One of the best probes of cosmological models is the Cosmic Microwave Background (CMB). The CMB is the radiation that was emitted during recombination when the Universe had cooled enough for electrons and protons to combine and not be ionised by the photon bath. While the CMB temperature looks isotropic on large scales, fluctuations around the average value of $T_{\mathrm{CMB}} \sim 2.73\,\mathrm{K}$ are observed at very small scales. These anisotropies are the result of oscillations in the baryonic matter known as Baryon Acoustic Oscillations (BAO). These oscillations were produced due to the interplay between the outward pressure caused by matter interactions and the pull of gravitation due to dark matter.

Measuring the angular power spectra of these anisotropies and fitting the cosmological parameters of the ΛCDM model tell us how the Universe's energy density

(Ω_{total}), is partitioned between the matter (Ω_{m}), radiation (Ω_{rad}), and dark energy (Ω_Λ) components. In a flat universe, of which we believe ours to be, these components should sum to $\Omega_{\text{tot}} = 1$. The Planck collaboration most recently performed a precise measurement of the CMB power spectrum in 2018, obtaining best-fit parameters

$$\Omega_{\text{m}} = 0.311 \pm 0.006, \quad \Omega_\Lambda = 0.689 \pm 0.006. \tag{1.4}$$

Combining the predicted baryon density from BBN with the CMB observations breaks down the matter abundance into the dark (Ω_{DM}) and baryonic (Ω_{b}) components yielding

$$\Omega_{\text{DM}}h^2 = 0.1193 \pm 0.0009, \quad \Omega_{\text{DM}}h^2 = 0.02242 \pm 0.00014, \tag{1.5}$$

where h is the dimensionless Hubble constant such that the Hubble parameter today is $H_0 = 100\,h\,\text{km}\,\text{s}^{-1}$ Mpc.

Large Scale Structure

After recombination, the pressure on the baryonic matter from photons subsided, allowing the small density perturbations to grow. This would lead to the growth of stars, galaxies and the large scale structure we observe today [10]. N-body simulations of the Universe's evolution require a cold dark matter component for this structure to form. While a small component of the dark matter can be warm, hot dark matter would wash out small scale structures [11].

1.2 Potential Models of Dark Matter

The general consensus amongst physicists is that dark matter has a particle nature, similar to the visible matter of the Standard Model. Models may be as simple as dark matter being described by a single field or there could be an extensive hidden sector with complicated symmetry structures. Given the few details we know about dark matter, there exists an enormous library of models that can produce a viable dark matter candidate. However, there are generic properties a good dark matter candidate must satisfy, namely:

- **Stable on Cosmological Timescales:** Dark matter must either be stable or have a lifetime significantly longer than the age of the Universe in order to be present in its current abundance.

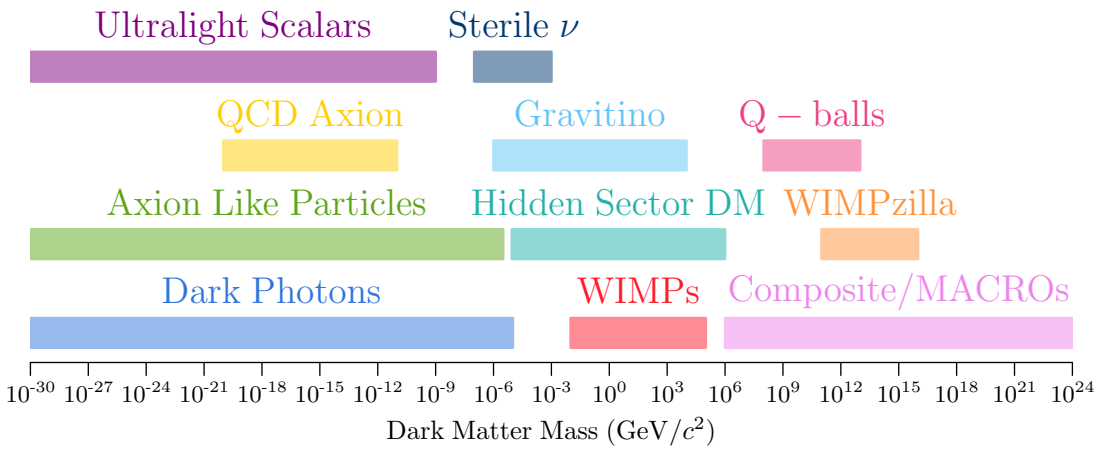

Figure 1.3: Illustrative landscape of dark matter models and the mass range for which they predict a valid candidate.

- **Neutral or milli-charged under Electromagnetism:** Dark matter, as its name suggests, does not significantly interact with light. By requiring that dark matter be completely decoupled from the Standard Model plasma by the time of recombination yields an upper bound on the milli-charge dark matter can carry of [12]

$$q_{\mathrm{DM}}/e < \begin{cases} 3.5 \times 10^{-7} \left(\frac{m_{\mathrm{DM}}}{1\,\mathrm{GeV}}\right)^{0.58}, & m_{\mathrm{DM}} > 1\,\mathrm{GeV} \\ 4.0 \times 10^{-7} \left(\frac{m_{\mathrm{DM}}}{1\,\mathrm{GeV}}\right)^{0.35}, & m_{\mathrm{DM}} < 1\,\mathrm{GeV}, \end{cases} \tag{1.6}$$

- **Small Self-Interactions:** The standard ΛCDM cosmology assumes that the dark matter is collisionless. However, small dark matter self-interactions can help resolve existing small-scale structure issues [13, 14]. Current limits on the self-interaction cross section are $\sigma_{\mathrm{DM-DM}}/m_{\mathrm{DM}} < 0.48\,\mathrm{cm}^2/\mathrm{g}$ come from merging galaxy clusters [15] and the ellipticity of galaxies obtained from X-ray observations [16].

A selection of the more prominent dark matter candidates is shown in Fig. 1.3. The key features of a few of these models are discussed below.

WIMPs

The Weakly Interacting Massive Particle (WIMP) is perhaps the most well-known dark matter candidate. WIMPs rose to fame thanks to the so-called "WIMP miracle" [17]. This refers to the fact that particles with weak scale masses and annihilation cross sections just so happen to have the correct relic abundance of dark

matter when produced via the freeze-out mechanism [18]. In this scenario, the final WIMP abundance depends on the total annihilation cross-section, $\langle \sigma v \rangle$, with only a very mild dependence on the DM mass [19],

$$\Omega_{\mathrm{DM}} h^2 \sim 0.12 \left(\frac{2.2 \times 10^{-26}\,\mathrm{cm}^3\,\mathrm{s}^{-1}}{\langle \sigma v \rangle} \right). \tag{1.7}$$

The canonical weak-scale WIMP has been tightly constrained from direct and indirect detection limits, leading it to be disfavoured as a dark matter candidate. The term "WIMP" is now typically used to refer to any particle dark matter candidate that is produced thermally in the early Universe. Such a particle can have a mass in the range $10\,\mathrm{MeV} \lesssim m_{\mathrm{WIMP}} \gtrsim 100\,\mathrm{TeV}$. Lighter WIMPs will have non-negligible contributions to the effective number of neutrino species, N_{eff}, which is constrained through BBN and the Cosmic Microwave Background CMB to be $N_{eff} = 2.99 \pm 0.17$ [20]. Masses larger than $\sim 100\,\mathrm{TeV}$ are excluded from partial wave unitarity [21].

Axions

The original axion was proposed by by Peccei and Quinn [22] as part of a dynamical solution to the "Strong CP Problem". This refers to the measured value of the neutron electric dipole moment (nEDM) being anomalously small, with a current upper bound of $|d_n| < 0.18 \times 10^{-26}\ e\,\mathrm{cm}$ [23]. This can be translated to an upper bound on the CP-violating QCD θ-parameter such that $|\theta_{QCD}| \lesssim 10^{-10}$, raising questions as to why this value seems to be fine-tuned to such a small value.

The Peccei-Quinn solution to this problem introduces a new, anomalous, global $U(1)_{\mathrm{PQ}}$ symmetry and promotes θ_{QCD} to be a dynamical field. The axion emerges as the pseudo-Goldstone boson associated with the breaking of $U(1)_{\mathrm{PQ}}$, such is in the two most prominent UV completions of the axion, the KSVZ [24, 25] and DFSZ [26, 27] models. In these models, the axion produced in the early Universe can serve the role of cold dark matter today. This makes it a very compelling dark matter candidate, as it solves two of the biggest mysteries of physics in one neat package.

However, solving the Strong CP problem can be rather restrictive on the model parameters. For example, the QCD axion's coupling to the photon is not a free parameter and depends on the scale at which the PQ symmetry is broken. Many models introduce a light pseudoscalar particle that is not associated with a solution to the Strong CP problem but has a coupling to the photon that takes the same form as the QCD axion. Such pseudoscalars are known as "Axion Like Particles" (ALPs) and can similarly make a good dark matter candidate.

Add some more candidates

1.2.1 Dark Matter in an Effective Fields Theory Framework

1.2.2 Overview of Effective Field Theory

Given the sheer quantity of potential dark matter models and candidates, a model-independent approach for analysing experimental results is often desired. An economical analysis method is to use an Effective Field Theory (EFT) to describe the dark matter-Standard Model interactions. Effective theories are prevalent in all of physics, e.g., describing light using ray optics vs Maxwell's equations or the orbits of planets using Newtonian gravity vs General relativity. The delineating factor in choosing a formalism is the scale (energy, length, etc.) we are interested in. **Add in the usual EFT diagram** Experiments will only be sensitive to interactions that can occur below some energy scale, i.e. 13.6 TeV at the LHC or 1 GeV in direct detection experiments; we are only interested in describing the interactions that occur below this scale.

One follows two main schools of thought when constructing an EFT. First, there is the *top down* approach. Here, you begin with a particular complete model in mind that consists of heavy and light fields. At energies below the production threshold of the heavy fields, these degrees of freedom can be "integrated out" of the theory. This process leaves an effective theory for the interactions among the light fields. The interactions that would be mediated by the heavy fields appear as non-renormalisable operators that are suppressed by this high energy scale, Λ.

The second method, known as the *bottom-up* approach, is more agnostic to the high-energy physics that might be in play. In this method, one constructs all possible operators that obey the required symmetries of the theory up to a desired mass dimension. Operators of mass dimension greater than four are then suppressed by powers the required number of powers of the high energy cutoff scale, Λ. This cutoff scale indicates the energy at which the EFT begins to break down and should at least be larger than the masses of the fields in the EFT. The Lagrangian constructed in this manner is made out of a tower of operators, $\mathcal{O}_i^{(n)}$, forming

$$\mathcal{L}_{\text{EFT}} \supset \sum_{n>4} \sum_{i=1}^{j_n} \frac{C_i^{(n)}}{\Lambda^{n-4}} \mathcal{O}_i^{(n)}, \tag{1.8}$$

where we sum over all j_n operators present at mass dimension n. The $C_i^{(n)}$ are called Wilson coefficients and are typically energy dependent.

In the context of dark matter, there are many EFTs describing the interaction at various energy scales. For example, dark matter scatting off nuclei in direct detection experiments is described by a non-relativistic EFT built out of the momentum transfer, relative velocity and spin operators of the dark matter and targets [28,

29]. At higher energy scales where relativistic effects become important, the EFT is instead constructed from relativistic fields, such as dark matter that may be produced in colliders.

Generally, an EFT will have fewer free parameters than the underlying UV theories, typically the dark matter mass and the high energy cutoff scale. This is in contrast with the dozens or so parameters often present in complete models. This allows for a simpler interpretation of experimental results as you will be fitting to a lower dimensional parameter space.

Move the next sections later?

1.2.3 Dimension 6 EFT Operators for Dirac Fermion Dark Matter

This work's approach will focus on dimension 6 EFT operators that describe the interactions of Dirac fermion dark matter with standard model fermions. These operators will have a structure

$$\mathcal{L}^{(6)}_{\text{EFT}} \sim \frac{1}{\Lambda^2}(\bar{\chi}\Gamma_\chi\chi)(\bar{f}\Gamma_{\text{SM}}f), \tag{1.9}$$

where the Γ_i determines the Lorentz structure of the interaction by taking appropriate combinations from the set

$$\Gamma_i \in \{1, i\gamma_5, \gamma^\mu, i\gamma^\mu\gamma^5, \sigma^{\mu\nu}, i\gamma^5\sigma^{\mu\nu}\}. \tag{1.10}$$

For example, the case of $\Gamma_\chi = \Gamma_{\text{SM}} = 1$ yields scalar currents for both the DM and SM fermions and would correspond to integrating out a heavy scalar mediator in the UV theory. There are 10 such operators at dimension six that form a linearly independent basis. These are given in Table 1.1, along with spin-averaged squared matrix element for dark matter scattering with a fermion. The coupling constants, g_f, are given in terms of the fermion Yukawa couplings, y_f, and the EFT cutoff scale, Λ_f. Hence, these operators describe interactions between dark matter and the elementary fermions of the Standard Model: the leptons and quarks.

1.2.4 Going from DM-Quark to DM-Nucleon Interactions

The operators in Table 1.1 describe dark matter interactions at the quark level, as these are the degrees of freedom most models are formulated with. However, we will primarily be interested in dark matter scattering with baryons, which requires taking the matrix element of the quark operators between baryon states,

Name	Operator	g_f	$\lvert\overline{M}(s,t,m_i)\rvert^2$
D1	$\bar{\chi}\chi\ \bar{f}f$	$\frac{y_f}{\Lambda_f^2}$	$g_f^2\frac{\left(4m_\chi^2-t\right)\left(4m_\chi^2-\mu^2 t\right)}{\mu^2}$
D2	$\bar{\chi}\gamma^5\chi\ \bar{f}f$	$i\frac{y_f}{\Lambda_f^2}$	$g_f^2\frac{t\left(\mu^2 t-4m_\chi^2\right)}{\mu^2}$
D3	$\bar{\chi}\chi\ \bar{f}\gamma^5 f$	$i\frac{y_f}{\Lambda_f^2}$	$g_f^2 t\left(t-4m_\chi^2\right)$
D4	$\bar{\chi}\gamma^5\chi\ \bar{f}\gamma^5 f$	$\frac{y_f}{\Lambda_f^2}$	$g_f^2 t^2$
D5	$\bar{\chi}\gamma_\mu\chi\ \bar{f}\gamma^\mu f$	$\frac{1}{\Lambda_f^2}$	$2g_f^2\frac{2\left(\mu^2+1\right)^2 m_\chi^4-4\left(\mu^2+1\right)\mu^2 s m_\chi^2+\mu^4\left(2s^2+2st+t^2\right)}{\mu^4}$
D6	$\bar{\chi}\gamma_\mu\gamma^5\chi\ \bar{f}\gamma^\mu f$	$\frac{1}{\Lambda_f^2}$	$2g_f^2\frac{2\left(\mu^2-1\right)^2 m_\chi^4-4\mu^2 m_\chi^2\left(\mu^2 s+s+\mu^2 t\right)+\mu^4\left(2s^2+2st+t^2\right)}{\mu^4}$
D7	$\bar{\chi}\gamma_\mu\chi\ \bar{f}\gamma^\mu\gamma^5 f$	$\frac{1}{\Lambda_f^2}$	$2g_f^2\frac{2\left(\mu^2-1\right)^2 m_\chi^4-4\mu^2 m_\chi^2\left(\mu^2 s+s+t\right)+\mu^4\left(2s^2+2st+t^2\right)}{\mu^4}$
D8	$\bar{\chi}\gamma_\mu\gamma^5\chi\ \bar{f}\gamma^\mu\gamma^5 f$	$\frac{1}{\Lambda_f^2}$	$2g_f^2\frac{2\left(\mu^4+10\mu^2+1\right)m_\chi^4-4\left(\mu^2+1\right)\mu^2 m_\chi^2(s+t)+\mu^4\left(2s^2+2st+t^2\right)}{\mu^4}$
D9	$\bar{\chi}\sigma_{\mu\nu}\chi\ \bar{f}\sigma^{\mu\nu}f$	$\frac{1}{\Lambda_f^2}$	$8g_f^2\frac{4\left(\mu^4+4\mu^2+1\right)m_\chi^4-2\left(\mu^2+1\right)\mu^2 m_\chi^2(4s+t)+\mu^4(2s+t)^2}{\mu^4}$
D10	$\bar{\chi}\sigma_{\mu\nu}\gamma^5\chi\ \bar{f}\sigma^{\mu\nu}f$	$\frac{i}{\Lambda_f^2}$	$8g_f^2\frac{4\left(\mu^2-1\right)^2 m_\chi^4-2\left(\mu^2+1\right)\mu^2 m_\chi^2(4s+t)+\mu^4(2s+t)^2}{\mu^4}$

Table 1.1: Dimension 6 EFT operators [30] for the coupling of Dirac DM to fermions (column 2), together with the squared matrix elements DM-fermion scattering (column 5), where s and t are Mandelstam variables, $\mu = m_\chi/m_T$, and m_T is the target mass.

i.e. $\langle\mathcal{B}|\bar{q}\,\Gamma_q q|\mathcal{B}\rangle$. These matrix elements can be calculated through the application of Chiral Perturbation Theory (ChPT), giving a baryon level EFT. The operators of this EFT will have the same form as those in Table 1.1, with the obvious replacement of $f \to \mathcal{B}$, as well as additional form factors that take into account the structure of the baryons.

The required form factors for each operator have been calculated at zero mo-

mentum transfer in Ref. [28] and are given by

$$c_{\mathcal{B}}^{S}(0) = \frac{2m_{\mathcal{B}}^2}{v^2}\left[\sum_{q=u,d,s} f_{T_q}^{(\mathcal{B})} + \frac{2}{9} f_{T_G}^{(\mathcal{B})}\right]^2, \tag{1.11}$$

$$c_{\mathcal{B}}^{P}(0) = \frac{2m_{\mathcal{B}}^2}{v^2}\left[\sum_{q=u,d,s} \left(1 - 3\frac{\overline{m}}{m_q}\right)\Delta_q^{(\mathcal{B})}\right]^2, \tag{1.12}$$

$$c_{\mathcal{B}}^{V}(0) = 9, \tag{1.13}$$

$$c_{\mathcal{B}}^{A}(0) = \left[\sum_{q=u,d,s} \Delta_q^{(\mathcal{B})}\right]^2, \tag{1.14}$$

$$c_{\mathcal{B}}^{T}(0) = \left[\sum_{q=u,d,s} \delta_q^{(\mathcal{B})}\right]^2, \tag{1.15}$$

where $v = 246$ GeV is the vacuum expectation value of the SM Higgs field, $\mathcal{B}$ is the baryonic species, $\overline{m} \equiv (1/m_u + 1/m_d + 1/m_s)^{-1}$ and $f_{T_q}^{(\mathcal{B})}$, $f_{T_G}^{(\mathcal{B})} = 1 - \sum_{q=u,d,s} f_{T_q}^{(\mathcal{B})}$, $\Delta_q^{(\mathcal{B})}$ and $\delta_q^{(\mathcal{B})}$ are the hadronic matrix elements, determined either experimentally or by lattice QCD simulations[1]. The specific values of these matrix elements for various baryons are provided in Appendix **ADD APPENDIX**.

These form factors are perfectly viable when considering interactions with momentum transfers $\lesssim 1\,\text{GeV}$ such as in direct detection experiments. For energies greater than this, the internal structure of the baryon begins to be resolved, and an additional momentum-dependent form factor is required to account for this [31],

$$F_{\mathcal{B}}(t) = \frac{1}{(1 - t/Q_0)^2}, \tag{1.16}$$

where t is the Mandelstam variable, and Q_0 is an energy scale that depends on the hadronic form factor. For simplicity, we will conservatively take $Q_0 = 1\,\text{GeV}$ for all operators. Putting everything together, the squared coupling constants for dark matter-baryon interactions are obtained by making the replacement

$$g_f^2 \to \frac{c_{\mathcal{B}}^{I}(t)}{\Lambda_q^4} \equiv \frac{1}{\Lambda_q^4} c_{\mathcal{B}}^{I}(0) F_{\mathcal{B}}^2(t), \quad I \in S, P, V, A, T, \tag{1.17}$$

in the matrix elements in the final column of Table 1.1.

[1] The superscript letters S, P, V, A and T stand for Scalar, Pseudoscalar, Vector, Axial-vector and Tensor interactions respectively. The corresponding operators are: D1-2 for S; D3-4 for P; D5-6 for V, D7-8 for A; and D9-10 for T.

1.3 Current Status of Dark Matter Constraints

In broad terms, there are three main ways that we can search for evidence of dark matter, often termed "make it, shake it or break it". "Make it" refers to dark matter being produced at colliders; "break it" to searching for dark matter annihilation signals; and "shake it" to direct detection of dark matter scattering. An illustrative way of depicting these processes is shown in Fig. **add usual diagram**. This section discusses the current status of these detection methods.

1.3.1 Collider Bounds

If dark matter is produced in a collider, it will simply leave the detector without depositing any energy. In order to determine if such an invisible particle was produced, conservation of energy-momentum is used to determine if there are any events that are missing energy. In practice, what is searched for is missing momentum that is transverse to the beamline.

Currently, dark matter has not been observed to be produced in particle colliders. This non-observation has instead been used to constrain the dark matter mass and production cross sections or couplings of various models. These limits are typically interpreted in a model-dependent manner, as different dark matter - Standard model couplings can significantly alter the production rates. As mentioned above, EFTs can be used to explore a variety of interactions in a somewhat model-independent way. However, many applications of this nature did not hold up to scrutiny, as the EFTs were being applied at energies outside their regions of validity [32–35], and so care is needed when applying such methods.

The ATLAS and CMS experiments at the LHC have performed analyses on various dark matter production mechanisms, including the exchange of a Z/Z' or Higgs, EFTs and heavy mediators, and mono-jet searches[2][36, 37]. Collider searches also offer complimentary probes of the dark matter-nucleon scattering cross-section [38].

It is important to note that an observation of an invisible massive particle at a collider is not enough to infer that it is dark matter. Such an observation only tells us that such a particle exists but nothing about its abundance, meaning it could just be a sub-component of a larger dark sector. In order to identify whether or not this was a dark matter detection, complimentary observations from direct or indirect detectors would be required.

[2]These searches refer to a single jet being produced alongside a pair of dark matter particles. This jet could be of Standard Model or dark sector origin, with the latter commonly referred to as "mono-X" searches.

1.3.2 Direct Detection Searches

Direct detection experiments vary wildly depending on the dark matter mass range they are trying to probe. For ALP dark matter that is wavelike, haloscope experiments such as ADMX [39] and MADMAX [40] attempt to convert ALPs to photons via the Primakoff effect. Searches for WIMP dark matter look for the dark matter scattering with some detector material, causing it to recoil and release some energy. Given our focus on WIMP dark matter, this section will review the experimental status of these detectors.

The differential rate in which the incoming flux of dark matter will scatter within a detector with N_T targets, as a function of the recoil energy, E_R, is given by

$$\frac{dR(E_R,t)}{dE_R} = N_T \frac{\rho_{\mathrm{DM}}}{m_{\mathrm{DM}}} \int_{v>v_{\mathrm{min}}}^{v_{\mathrm{esc}}} v f(\vec{v}+\vec{v}_E) \frac{d\sigma}{dE_R} d^3v, \tag{1.18}$$

and depends on the quantities:

- v_{min} is the minimum dark matter velocity required by kinematics for a scattering event to occur;
- $v_{\mathrm{esc}} = 528\,\mathrm{km\,s^{-1}}$ is the Milky Way escape velocity;
- $\vec{v}_E$ is the velocity of the Earth through the dark matter halo[3];
- $f(\vec{v}-\vec{v}_E)$ is the dark matter velocity distribution in the Earth's frame;
- $d\sigma/dE_R$ is the differential scattering cross-section.

Given the low interaction rate of dark matter, the expected event rate in detectors is very low, around one event per day, per kilogram of target material, per kiloelectronvolt deposited. Having such a low event rate requires the detector to be situated in an extremely low background environment, such as underground laboratories.

Direct detection experiments aim to probe two main types of dark matter interactions: spin-dependent (SD) and spin-independent (SI) scattering. SD interactions couple to the overall spin of the target, while SI interactions are agnostic to this. Therefore, experiments searching for SI interactions benefit from using nuclei with a large atomic number, A, as the interaction cross-section will involve a coherent sum over all nucleons. This leads to an A^2 enhancement of SI interactions compared to SD ones.

[3] This accounts for the orbit of the Earth around the Sun, which induces an annual modulation in the flux of DM.

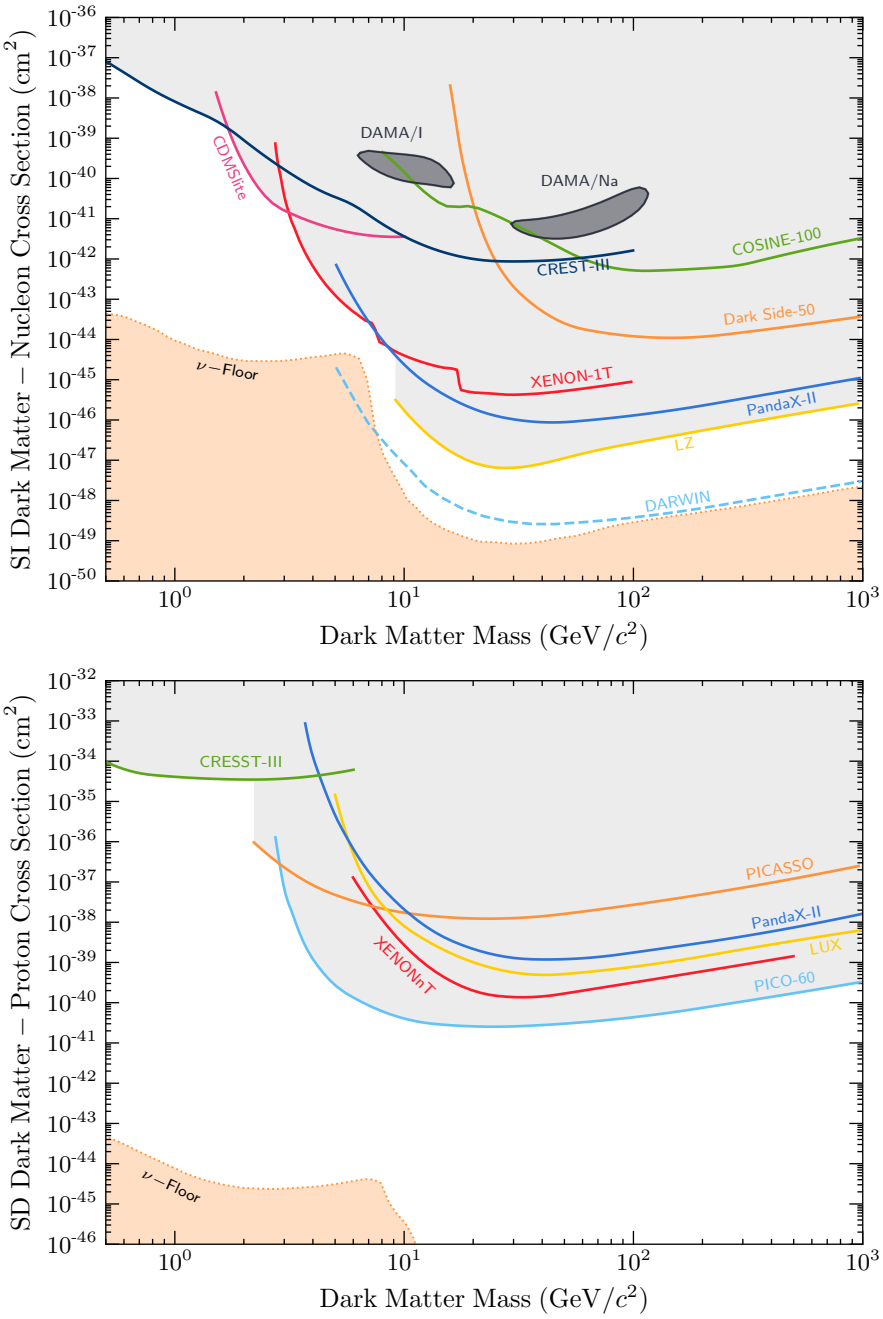

Figure 1.4: Current status of direct detection searches for dark matter. **Top:** Spin-independent dark matter-nucleon scattering. **Bottom:** Spin-dependent dark matter-proton scattering.

The current leading constraints on the dark matter-nucleon scattering cross-section are shown in Fig. 1.4, with SI in the top panel and SD in the bottom. The SI limits come from the liquid noble gas experiments (LZ [41], XENON-1T [42], PandaX-II [43], and DarkSide-50 [44]), solid-state cryogenic detectors (CRESST-III [45], and CDMSlite [46]), and room temperature crystals (DAMA/LIBRA [47], and COSINE-100 [48]).

The SD experiments require their targets to carry non-zero spin for the dark matter to couple to. ^{19}F is the favourable choice proton scattering, as it has an unpaired proton giving it its overall spin. The leading constraints come from superheated liquid experiments such as the PICO-60 [49] as well as PICASSO [50] In terms of the SD proton scattering shown in Fig 1.4, These interations are also searched for by many of the same experiments in the SI case, with the inclusion of LZ's predecessor LUX [51].

neutrino floor

shortfalls: min thresholds, decreas sensitity to hogher masses

1.3.3 Indirect Detection

It is this route that we will follow to explore dark matter EFTs.

1.4 Compact Objects as Dark Matter Probes

Compact objects, namely Neutron Stars and White Dwarfs, offer a unique laboratory for studying dark matter interactions. Their extreme environments offer many benefits in comparison to direct detection experiments. These include:

- **Gravitational focusing of the DM flux.** In the NS case, the infalling DM will be boosted to semi-relativistic velocities ($\sim 0.2 - 0.7c$ depending on the NS mass).
-

We will study each operator in isolation, i.e. consider a Lagrangian that contains only one of the operators, rather than a linear superposition of multiple. This way, we can analyse specific types of interactions independently, allowing us to take as model-independent an approach to phenomenology as possible.

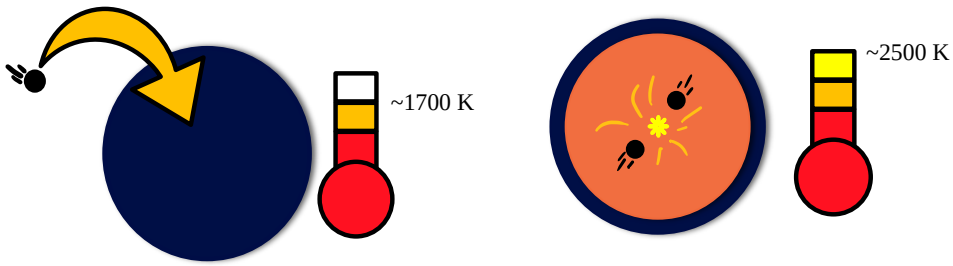

Figure 1.5: Illustration of DM-induced heating of compact objects. **Left:** kinetic heating due to DM scattering, raising the temperature to $\sim 1700\,\mathrm{K}$. **Right:** further annihilation heating adding an additional $\sim 800\,\mathrm{K}$.

2

Compact Objects for Particle Physics

Introduce COs, formation, structure etc...

Check masses in Shapiro

The lifecycle of main sequence stars can end in various ways depending on the progenitor star's mass. Lighter stars ($0.6-10M_{\odot}$ at the onset of hydrogen burning) will eventually end their lives as a White Dwarf. Meanwhile,

2.1 Internal structure

In this thesis we will only be considering spherically symmetric and static stars. The internal structure of

For non-relativistic stars, such as our Sun, the structure equations are rather simple, them being

$$\frac{dM}{dr} = 4\pi r^2, \tag{2.1}$$

$$\frac{dP}{dr} = -\rho(r)GM(r)r^2, \tag{2.2}$$

where M is the mass of the star at radius r, P is the pressure, and $\rho(r)$ is the density. The first equation is known as the mass equation, and the second is the condition for hydrostatic equilibrium.

We are instead interested in compact objects, where the extreme densities of these stars

In order to solve this system, The equation of state describes the relation between the pressure and energy of the constituent matter.

2.1.1 White Dwarfs

FMT equation of state

2.1.2 Neutron Stars

Beta Equlibrium

2.2 Observational Status

2.2.1 White Dwarfs

2.2.2 Neutron Stars

3
Capture Part 1: Point Like Targets

Review capture in the Sun, move to what's needed for COs in general, then specify to WDs (ions + electrons) and NS (interacting baryons)

One of the most essential quantities we will be interested in is the the rate at which dark matter is captured with the star. In this chapter, we focus on building up the formalism of dark matter capture within compact objects, outlining how this differs from the the standard calculation for capture in the Sun. We restrict our analysis to scattering off of point-like targets relevant for leptonic species, i.e. electrons in White Dwarfs and electrons and muons in Neutron Stars. The complications that arise due to the finite size of hadronic targets will be discussed in the next chapter.

3.1 Dark Matter Capture in the Sun

Before jumping into the capture formalism relevant to compact objects, it will serve us well to review the formalism laid out by Gould for capture in the Sun [52, 53].

To begin, we consider the flux of dark matter particles that pass through a spherical shell a large distance R from the star, where the gravitational field is negligible. For this, we need to know the distribution function of the relative velocity between the DM and the stellar constituents. The velocity distribution function will be spatially isotropic, and so for simplicity we will assume that the

DM follows a Maxwell-Boltzmann distribution function,

$$f_\infty(\tilde{u}_\chi)d\tilde{u}_\chi = 4\pi\left(\frac{3}{2\pi}\right)^{3/2}\frac{\tilde{u}_\chi^2}{v_d^2}\exp\left(-\frac{3\tilde{u}_\chi^2}{2v_d^3}\right)d\tilde{u}_\chi, \tag{3.1}$$

where $\tilde{u}_\chi$ is the DM velocity in the halo, and v_d is the DM halo velocity dispersion.

Taking into account the motion of the star through the halo and the thermal motion of the constituents, which are assumed to follow a Maxwell-Boltzmann distribution, gives the relative velocity between the DM and targets, u_χ. The distribution function for the relative velocity can be expressed as [54]

$$f_{\rm MB}(u_\chi)du_\chi = \frac{u_\chi}{v_\star}\sqrt{\frac{3}{2\pi(v_d^2+3T_\star/m_T)}}\left(e^{-\frac{3(u_\chi-v_\star)^2}{2(v_d^2+3T_\star/m_T)}}-e^{-\frac{3(u_\chi+v_\star)^2}{2(v_d^2+3T_\star/m_T)}}\right), \tag{3.2}$$

where $v_\star$ is the star's velocity in the halo rest frame[1], $T_\star$ is the temperature of the star, and m_T is the mass of the target.

Returning to the large spherical shell of radius R, given the velocity distribution function, we can obtain the flux of DM through this surface. The rate of DM particles passing through a surface element $d\tilde{A}$ with velocity between u_χ and $u_\chi + du_\chi$, with an angle to the normal of $d\tilde{A}$ between $\tilde{\theta}$ and $\tilde{\theta}+d\tilde{\theta}$ and an azimuthal angle between $\tilde{\phi}$ and $\tilde{\phi}+d\tilde{\phi}$ is given by [55]

$$\frac{dN_\chi}{dt} = \frac{\rho_\chi}{m_\chi}f_{\rm MB}(u_\chi)\vec{u}\cdot d\vec{\tilde{A}}\,du_\chi\,\frac{d\tilde{\Omega}}{4\pi} \tag{3.3}$$

$$= \frac{\rho_\chi}{m_\chi}f_{\rm MB}(u_\chi)u_\chi\cos\tilde{\theta}\,d\tilde{A}\,du_\chi\,\frac{d\cos\tilde{\theta}\,d\tilde{\phi}}{4\pi} \tag{3.4}$$

$$= \frac{1}{4}\frac{\rho_\chi}{m_\chi}f_{\rm MB}(u_\chi)u_\chi d\tilde{A}\,du_\chi\,d\cos^2\tilde{\theta}, \tag{3.5}$$

where we have integrated over the azimuthal angle $\tilde{\phi}$ due to the isotropy of the system. The number density of the DM is included through the ρ_χ/m_χ factor. Integrating over the area of the sphere is trivial due to isotropy, leaving us with

$$\frac{dN_\chi}{dt} = \pi\frac{\rho_\chi}{m_\chi}f(u_\chi)u_\chi\,du_\chi\,d\cos^2\tilde{\theta}, \tag{3.6}$$

with the integration interval for $\cos^2\tilde{\theta}$ being $(0,1)$.

As the DM begins to infall from this large distance R to a closer distance r, the star's gravitational field will boost the velocity by the local escape velocity $v_e(r)$

[1] This is the frame where the DM has an average velocity of zero.

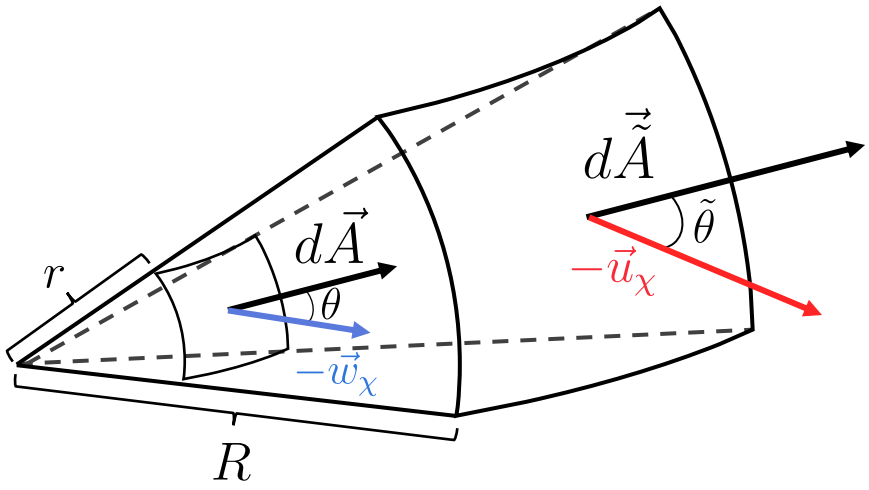

Figure 3.1: Geometry of the capture process. The azimuthal angles are not shown for simplicity as they can be integrated over trivially.

such that

$$w_\chi^2(r) = u_\chi^2 + v_e^2(r), \tag{3.7}$$

$$v_e^2(r) = \frac{2GM_\star}{R_\star} + \int_r^{R_\star} \frac{GM_\star(r')}{r'^2}\, dr'. \tag{3.8}$$

Due to the conservation of angular momentum, we can relate the angular momentum of the DM at the two distances R and r such that

$$J_\chi = m_\chi R u_\chi \sin\tilde{\theta} = m_\chi r w_\chi(r) \sin\theta \leq m_\chi r w_\chi(r) \equiv J_{\max}, \tag{3.9}$$

where θ is the incident angle of the DM at the closer distance r, and we have defined the maximum angular momentum $J_{\max}$ corresponding to a linear DM trajectory.

Changing integration variables from $\cos^2\tilde{\theta}$ to J_χ allows us to write the number of DM particles passing through the shell per unit volume as

$$\frac{dN_\chi}{dt} = 2\pi \frac{\rho_\chi}{m_\chi} \frac{f_{\rm MB}(u_\chi)}{u_\chi} r^2 w_\chi^2(r) \frac{J_\chi dJ_\chi}{J_{\max}^2}\, du_\chi. \tag{3.10}$$

The geometry of the system is shown in Fig. 3.1 for clarity.

The probability that the DM interacts with the constituents of the shell depends on the interaction rate, $\Omega(w_\chi)$, multiplied by the time spent in the shell, $dt = dr/\dot{r}$.

Hence, the probability of scattering within the shell is

$$\Omega(w_\chi)\frac{dr}{\dot{r}} = 2\Omega(w_\chi)\frac{1}{w_\chi}\left(1-\left(\frac{J_\chi}{rw_\chi}\right)^2\right)^{-1/2}\Theta(J_{\max}-J_\chi)\,dr, \tag{3.11}$$

where the factor of 2 is due to the DM having two opportunities to pass through the shell, once when incoming and another after turning around[2]. The step-function is put in to ensure the angular momentum does not exceed its maximum allowed value.

For a scattered DM to be considered captured, it must lose enough energy in the collision to become gravitationally bound. The rate at which a DM particle scatters from an initial velocity w_χ to a final velocity $v < v_e(r)$ is given by [52–54]

$$\Omega^-(w_\chi) = \int_0^{v_e} R^-(w_\chi \to v)dv, \tag{3.12}$$

$$R^-(w_\chi \to v) = \int n_T(r)\frac{d\sigma_{\chi T}}{dv}|\vec{w}_\chi - \vec{u}_T|f_T(u_T)\,d^3\vec{u}_T, \tag{3.13}$$

with $R^-(w_\chi \to v)$ being the differential interaction rate, n_T is the target number density, u_T is the target velocity and $f_T(u_T)$ is the corresponding distribution function, and $d\sigma_{\chi T}/dv$ is the differential cross-section. The minus superscript is used to signify that this is the down scattering rate, i.e. the rate of interactions leading to the DM losing energy.

Finally, we obtain the capture rate by multiplying Eqs. 3.10 and 3.11 and integrate over the angular momentum to give the result

$$C = \int_0^{R_\star} dr\,4\pi r^2 \int_0^\infty du_\chi \frac{\rho_\chi}{m_\chi}\frac{f_{\rm MB}(u_\chi)}{u_\chi}w_\chi(r)\Omega^-(w_\chi). \tag{3.14}$$

This result is rather generic, as the choice of DM model will only dictate the form of the differential cross section in Eq. 3.13. In fact, as written above, the distribution function for the relative velocity far from the star can be any isotropic distribution function. The MB form was chosen as it allows for a simple analytic form.

3.2 Capture in Compact Objects

Having reviewed the capture process in non-relativistic stars, we can begin discussing the necessary modifications required when considering relativistic stars. In this section, we consider the two major modifications that need to be made:

[2]The radial velocity $\dot{r}$ is a standard result in orbital mechanics and can be obtained from the central force Lagrangian.

- The corrections from General Relativity due to the extreme gravitational fields. This ultimately alters the flux of DM passing through the star, boosting it through gravitational focusing.

- Accounting for the relativistic and degenerate nature of the star's constituents in the interaction rate.

The former is generic to neutron stars and white dwarfs, while the latter is required for all NS constituents, but only the electrons in a WD are degenerate and relativistic. The ions of the WD are non-relativistic and non-degenerate and, hence, can be treated the same as the Sun's constituents.

3.2.1 General Relativistic Corrections to the Capture Rate

Far from the star, the physics is the same as in the previous section. The deviations arise as the DM falls into he gravitational potential of the star. We begin by following the DM along its trajectory, moving from a distance $R \gg R_\star$ to a closer distance r. Hence, we are working in the DM rest frame and calculating the rate at which the DM passes through the shell *per unit of proper time*, τ. The proper time interval is related to the metric through

$$d\tau^2 = B(r)dt^2 - A(r)dr^2 - r^2 d\Omega^2, \tag{3.15}$$

with $B(r)$ and $A(r)$ defined in Chapter 2.

Following the same arguments as in the non-relativistic case, the flux of DM passing through the shell is

$$\frac{dN_\chi}{d\tau} = 2\pi \frac{\rho_\chi}{m_\chi} \frac{f_{\rm MB}(u_\chi)}{u_\chi} du_\chi \frac{J_\chi dJ_\chi}{m_\chi^2}, \tag{3.16}$$

which takes the same form as Eq. 3.10, with the physical difference being that this is the rate with respect to the proper time.

The probability that DM scatters within the shell and is captured is $2\hat{\Omega}^-(r)d\tau$, where $\hat{\Omega}^-(r)$ is the interaction rate with respect to the proper time, and $d\tau$ is the proper time taken to move from coordinate r to $r + dr$. The factor of 2 once again accounts for the DM crossing the shell twice per orbit. For calculation purposes, we need to relate this to the interaction rate seen by a distant observer, $\Omega^-(r)$, that is done through

$$\hat{\Omega}^-(r)d\tau = \frac{1}{\sqrt{g_{tt}}}\Omega^-(r)d\tau = \frac{1}{\sqrt{B(r)}}\Omega^-(r)d\tau. \tag{3.17}$$

Now, the proper time that the DM spends inside a shell of thickness dr will be[3]

$$d\tau = \left(\frac{d\tau}{dt}\right) dt = B(r)\frac{dr}{\dot{r}} = \frac{\sqrt{B(r)}dr}{\sqrt{\frac{1}{A(r)}\left[1 - B(r)\left(1 + \frac{J_\chi^2}{m_\chi^2 r^2}\right)\right]}}. \tag{3.18}$$

Combining everything together gives us the differential capture rate,

$$dC = 2\pi \frac{\rho_\chi}{m_\chi} \frac{f_{\rm MB}(u_\chi)}{u_\chi}\, du_\chi\, \frac{dJ_\chi^2}{m_\chi^2} \frac{\Omega^-(r)\sqrt{A(r)}\, dr}{\sqrt{1 - B(r)\left(1 + \frac{J_\chi^2}{m_\chi^2 r^2}\right)}}. \tag{3.19}$$

As the total number of targets in the star, N_T, needs to satisfy

$$N_T = \int_0^{R_\star} 4\pi r^2 n_T(r)\sqrt{A(r)}\, dr, \tag{3.20}$$

where $n_T(r)$ is the number density that appears in the interaction rate, we absorb the factor $\sqrt{A(r)}$ into the definition of $n_T(r)$, such that $\Omega^-(r)\sqrt{A(r)} \to \Omega^-(r)$. This is due to the number densities obtained by solving the TOV equations already account for the $\sqrt{A(r)}$ factor.

As before, we have $w_\chi^2(r) = u_\chi^2 + v_e^2(r)$, however as the escape velocity will be significantly larger than the ambient DM velocity far from the star, we can safely approximate $w_\chi^2(r) \approx v_e^2(r)$. In the relativistic case, the escape velocity can be defined as

$$v_e^2(r) = \left(\frac{dl}{d\tau}\right)^2 = A(r)\left(\frac{dr}{d\tau}\right)^2 + r^2\left(\frac{d\phi}{d\tau}\right)^2 = 1 - B(r), \tag{3.21}$$

where dl is a length element. The large boost from the escape velocity also removes the u_χ dependence in the kinematics of the interactions and allows us to perform the integration over the initial DM velocity, yielding an overall factor of

$$\int_0^\infty \frac{f_{\rm MB}(u_\chi)}{u_\chi} du_\chi = \frac{1}{v_\star}\,\mathrm{Erf}\left(\sqrt{\frac{3}{2}}\frac{v_\star}{v_d}\right). \tag{3.22}$$

To integrate over J_χ^2, we need the maximum angular momentum the DM can achieve as it passes through the shell. This can be obtained by requiring the argument of the radical above to remain positive, giving

$$J_{\rm max} = \sqrt{\frac{1 - B(r)}{B(r)}} m_\chi r. \tag{3.23}$$

[3]See Appendix **??** for the derivation of $\dot{r} = \frac{dr}{dt}$.

The factor of $1/\sqrt{B}$ arises due to the gravitational focusing of the incoming flux of DM [56].

Putting everything together, and integrating over the radius of the star, we are left with the final result for the capture rate of

$$C = \frac{4\pi}{v_\star}\frac{\rho_\chi}{m_\chi}\,\mathrm{Erf}\left(\sqrt{\frac{3}{2}}\frac{v_\star}{v_d}\right)\int_0^{R_\star} r^2\frac{\sqrt{1-B(r)}}{B(r)}\Omega^-(r)\,dr. \tag{3.24}$$

3.2.2 Interaction Rate for Degenerate Targets

3.3 White Dwarfs: Electron Targets

3.4 Neutron Stars: Leptoinc Targets

4

Capture Rate for Strongly Interacting Baryonic Matter

The capture formalism developed in the previous chapter is extended to baryonic targets inside neutron stars. Additional complications arise due to their finite size and strong interactions between the baryonic species.

5

Dark Matter Induced Heating of Neutron Stars

We analyse the various timescales at play when determining the extent of heating dark matter can induce in neutron stars. This heating occurs in two stages. Kinetic heating requires a significant fraction of the dark matter's kinetic energy to be deposited through scattering. Further annihilation heating requires the captures and annihilation rates to come into equilibrium. The timescales for these processes is calculated and compared to the age of the star.

5.1 Thermalisation Time

5.2 Capture-Annihilation Equilibrium

5.3 Dark Matter Heating

5.3.1 Kinetic Heating

5.3.2 Annihilation Heating

6
Conclusion

Concluding remarks

A
Kinematics

Derivation of $E_f^{'}$ as needed for capture and other kinematics

Definition of Symbols and Abbreviations

$\boldsymbol{C}_{\text{geo}}$ Geometric Capture Rate

DM Dark Matter
$\boldsymbol{K}_{\chi}$ Dark Matter Kinetic Energy
$\boldsymbol{\rho}_{\chi}$ DM halo density
$\boldsymbol{m}_{\chi}$ Dark Matter Mass

EFT Effective Field Theory
EoS Equation of State

$\boldsymbol{f}_{\text{FD}}$ Fermi-Dirac Distribution
$\boldsymbol{\varepsilon}_{F,i}$ Fermi kinetic energy of target species

$\boldsymbol{|\overline{\mathcal{M}}|^2}$ Spin-averaged squared matrix element
$\boldsymbol{\mu}$ DM-Target mass ratio, m_{χ}/m_i

NS Neutron Star

PB Pauli Blocking

QMC Quark-Meson-Coupling EoS

$\boldsymbol{\sigma_{\text{th}}}$ Threshold Cross Section

$\boldsymbol{T}_{\text{eq}}$ Equilibrium Temperature
$\boldsymbol{t}_{\text{eq}}$ Capture-Annihilation equilibrium time
$\boldsymbol{T}_{\star}$ Temperature of the star
$\boldsymbol{t}_{\text{therm}}$ Thermalisation time

$\boldsymbol{v}_d$ DM halo dispersion velocity
$\boldsymbol{v}_{\star}$ Star velocity

Bibliography

[1] Nicole F. Bell et al. "Improved Treatment of Dark Matter Capture in Neutron Stars". In: *JCAP* 09 (Sept. 15, 2020), p. 028. DOI: 10.1088/1475-7516/2020/09/028. arXiv: 2004.14888 [hep-ph].

[2] Nicole F. Bell et al. "Improved Treatment of Dark Matter Capture in Neutron Stars II: Leptonic Targets". In: *JCAP* 03 (Mar. 26, 2021), p. 086. DOI: 10.1088/1475-7516/2021/03/086. arXiv: 2010.13257 [hep-ph].

[3] Nicole F. Bell et al. "Nucleon Structure and Strong Interactions in Dark Matter Capture in Neutron Stars". In: *Phys. Rev. Lett.* 127.11 (Sept. 10, 2021), p. 111803. DOI: 10.1103/PhysRevLett.127.111803. arXiv: 2012.08918 [hep-ph].

[4] Nicole F. Bell et al. "Improved Treatment of Dark Matter Capture in White Dwarfs". In: *JCAP* 10 (Oct. 29, 2021), p. 083. DOI: 10.1088/1475-7516/2021/10/083. arXiv: 2104.14367 [hep-ph].

[5] Filippo Anzuini et al. "Improved Treatment of Dark Matter Capture in Neutron Stars III: Nucleon and Exotic Targets". In: *JCAP* 11.11 (Nov. 29, 2021), p. 056. DOI: 10.1088/1475-7516/2021/11/056. arXiv: 2108.02525 [hep-ph].

[6] Nicole F. Bell et al. "Thermalization and Annihilation of Dark Matter in Neutron Stars". In: *arXiv:2312.11892 [hep-ph]* (Dec. 2023). arXiv: 2312.11892 [hep-ph].

[7] F. Zwicky. "On the Masses of Nebulae and of Clusters of Nebulae". In: *The Astrophysical Journal* 86 (1937), pp. 217–246. DOI: 10.1086/143864.

[8] Katherine Freese. "Review of Observational Evidence for Dark Matter in the Universe and in Upcoming Searches for Dark Stars". In: *EAS Publications Series* 36 (May 30, 2009), pp. 113–126. DOI: 10.1051/eas/0936016. arXiv: 0812.4005 [astro-ph].

[9] Federico Lelli, Stacy S. McGaugh, and James M. Schombert. "SPARC: Mass Models for 175 Disk Galaxies with Spitzer Photometry and Accurate Rotation Curves". In: *The Astronomical Journal* 152.6 (2016), p. 157. DOI: 10.3847/0004-6256/152/6/157. arXiv: 1606.09251 [astro-ph.GA].

[10] Volker Springel, Carlos S. Frenk, and Simon D. M. White. "The Large-Scale Structure of the Universe". In: *Nature* 440.7088 (2006), p. 1137. DOI: 10.1038/nature04805. arXiv: astro-ph/0604561.

[11] Volker Springel et al. "Simulating the Joint Evolution of Quasars, Galaxies and Their Large-Scale Distribution". In: *Nature* 435.7042 (2005), pp. 629–636. DOI: 10.1038/nature03597. arXiv: astro-ph/0504097.

[12] Samuel D. McDermott, Hai-Bo Yu, and Kathryn M. Zurek. "Turning off the Lights: How Dark Is Dark Matter?" In: *Physical Review D* 83.6 (2011), p. 063509. DOI: 10.1103/PhysRevD.83.063509. arXiv: 1011.2907 [hep-ph].

[13] Sean Tulin and Hai-Bo Yu. "Dark Matter Self-interactions and Small Scale Structure". In: *Physics Reports* 730 (Feb. 5, 2018), pp. 1–57. DOI: 10.1016/j.physrep.2017.11.004. arXiv: 1705.02358 [hep-ph].

[14] David N. Spergel and Paul J. Steinhardt. "Observational Evidence for Self-Interacting Cold Dark Matter". In: *Physical Review Letters* 84.17 (2000), pp. 3760–3763. DOI: 10.1103/PhysRevLett.84.3760. arXiv: astro-ph/9909386.

[15] Scott W. Randall et al. "Constraints on the Self-Interaction Cross-Section of Dark Matter from Numerical Simulations of the Merging Galaxy Cluster 1E 0657-5". In: *The Astrophysical Journal* 679.2 (2008), pp. 1173–1180. DOI: 10.1086/587859. arXiv: 0704.0261 [astro-ph].

[16] David A. Buote et al. "Chandra Evidence for a Flattened, Triaxial Dark Matter Halo in the Elliptical Galaxy NGC 720". In: *The Astrophysical Journal* 577.1 (2002), pp. 183–196. DOI: 10.1086/342158. arXiv: astro-ph/0205469.

[17] Jonathan L. Feng. "Dark Matter Candidates from Particle Physics and Methods of Detection". In: *Ann. Rev. Astron. Astrophys.* 48 (2010), pp. 495–545. DOI: 10.1146/annurev-astro-082708-101659. arXiv: 1003.0904 [astro-ph.CO].

[18] Gerard Jungman, Marc Kamionkowski, and Kim Griest. "Supersymmetric Dark Matter". In: *Phys. Rept.* 267 (1996), pp. 195–373. DOI: 10.1016/0370-1573(95)00058-5. arXiv: hep-ph/9506380.

[19] Gary Steigman, Basudeb Dasgupta, and John F. Beacom. "Precise Relic WIMP Abundance and Its Impact on Searches for Dark Matter Annihilation". In: *Phys. Rev. D* 86 (2012), p. 023506. DOI: 10.1103/PhysRevD.86.023506. arXiv: 1204.3622 [hep-ph].

[20] N. Aghanim, Y. Akrami, M. Ashdown, et al. "Planck 2018 Results. VI. Cosmological Parameters". In: *Astronomy & Astrophysics* 641 (Sept. 1, 2020), A6. DOI: 10.1051/0004-6361/201833910. arXiv: 1807.06209 [astro-ph.CO].

[21] Kim Griest and Marc Kamionkowski. "Unitarity Limits on the Mass and Radius of Dark Matter Particles". In: *Phys. Rev. Lett.* 64 (1990), p. 615. DOI: 10.1103/PhysRevLett.64.615.

[22] R. D. Peccei and Helen R. Quinn. "CP Conservation in the Presence of Instantons". In: *Phys. Rev. Lett.* 38 (1977), pp. 1440–1443. DOI: 10.1103/PhysRevLett.38.1440.

[23] C. Abel et al. "Measurement of the Permanent Electric Dipole Moment of the Neutron". In: *Phys. Rev. Lett.* 124.8 (Feb. 29, 2020), p. 081803. DOI: 10.1103/PhysRevLett.124.081803. arXiv: 2001.11966 [hep-ex].

[24] Jihn E. Kim. "Weak Interaction Singlet and Strong CP Invariance". In: *Phys. Rev. Lett.* 43 (1979), p. 103. DOI: 10.1103/PhysRevLett.43.103.

[25] Mikhail A. Shifman, A. I. Vainshtein, and Valentin I. Zakharov. "Can Confinement Ensure Natural CP Invariance of Strong Interactions?" In: *Nucl. Phys. B* 166 (1980), pp. 493–506. DOI: 10.1016/0550-3213(80)90209-6.

[26] A. R. Zhitnitsky. "On Possible Suppression of the Axion Hadron Interactions. (In Russian)". In: *Sov. J. Nucl. Phys.* 31 (1980), p. 260.

[27] Michael Dine, Willy Fischler, and Mark Srednicki. "A Simple Solution to the Strong CP Problem with a Harmless Axion". In: *Phys. Lett. B* 104 (1981), pp. 199–202. DOI: 10.1016/0370-2693(81)90590-6.

[28] Eugenio Del Nobile, Marco Cirelli, and Paolo Panci. "Tools for Model-Independent Bounds in Direct Dark Matter Searches". In: *Journal of Cosmology and Astroparticle Physics* 10.10 (Oct. 10, 2013), p. 019. DOI: 10.1088/1475-7516/2013/10/019. arXiv: 1307.5955 [hep-ph].

[29] A. Liam Fitzpatrick et al. "The Effective Field Theory of Dark Matter Direct Detection". In: *Journal of Cosmology and Astroparticle Physics* 02.02 (2013), p. 004. DOI: 10.1088/1475-7516/2013/02/004. arXiv: 1203.3542 [hep-ph].

[30] Jessica Goodman et al. "Constraints on Dark Matter from Colliders". In: *Physical Review D* 82.11 (2010), p. 116010. DOI: 10.1103/PhysRevD.82.116010. arXiv: 1008.1783 [hep-ph].

[31] "Electromagnetic Structure of the Nucleon". In: *The Structure of the Nucleon*. John Wiley & Sons, Ltd, 2001, pp. 7–51. DOI: 10.1002/352760314X.ch2.

[32] Giorgio Busoni et al. "On the Validity of the Effective Field Theory for Dark Matter Searches at the LHC". In: *Phys. Lett. B* 728 (Jan. 20, 2014), pp. 412–421. DOI: 10.1016/j.physletb.2013.11.069. arXiv: 1307.2253 [hep-ph].

[33] O. Buchmueller, Matthew J. Dolan, and Christopher McCabe. "Beyond Effective Field Theory for Dark Matter Searches at the LHC". In: *JHEP* 01 (2014), p. 025. DOI: 10.1007/JHEP01(2014)025. arXiv: 1308.6799 [hep-ph].

[34] Giorgio Busoni et al. “On the Validity of the Effective Field Theory for Dark Matter Searches at the LHC Part III: Analysis for the t-Channel”. In: *JCAP* 09 (2014), p. 022. DOI: 10.1088/1475-7516/2014/09/022. arXiv: 1405.3101 [hep-ph].

[35] Giorgio Busoni et al. “On the Validity of the Effective Field Theory for Dark Matter Searches at the LHC, Part II: Complete Analysis for the s-Channel”. In: *JCAP* 06 (2014), p. 060. DOI: 10.1088/1475-7516/2014/06/060. arXiv: 1402.1275 [hep-ph].

[36] Albert M Sirunyan, Armen Tumasyan, Wolfgang Adam, et al. “Search for Dark Matter Produced with an Energetic Jet or a Hadronically Decaying W or Z Boson at Sqrt(s) = 13 TeV”. In: *Journal of High Energy Physics* 07.7 (July 5, 2017), p. 014. DOI: 10.1007/JHEP07(2017)014. arXiv: 1703.01651 [hep-ex].

[37] Albert M Sirunyan, Armen Tumasyan, Wolfgang Adam, et al. “Search for Dark Matter Produced with an Energetic Jet or a Hadronically Decaying W or Z Boson at Sqrt(s) = 13 TeV”. In: *Journal of High Energy Physics* 07.7 (July 5, 2017), p. 014. DOI: 10.1007/JHEP07(2017)014. arXiv: 1703.01651 [hep-ex].

[38] F. Ruppin et al. “Complementarity of Dark Matter Detectors in Light of the Neutrino Background”. In: *Physical Review D* 90.8 (Oct. 7, 2014), p. 083510. DOI: 10.1103/PhysRevD.90.083510. arXiv: 1408.3581 [hep-ph].

[39] S. J. Asztalos et al. “A SQUID-based Microwave Cavity Search for Dark-Matter Axions”. In: *Phys. Rev. Lett.* 104 (2010), p. 041301. DOI: 10.1103/PhysRevLett.104.041301. arXiv: 0910.5914 [astro-ph.CO].

[40] P. Brun, A. Caldwell, L. Chevalier, et al. “A New Experimental Approach to Probe QCD Axion Dark Matter in the Mass Range above 40μeV”. In: *The European Physical Journal C* 79.3 (Mar. 2019), p. 186. DOI: 10.1140/epjc/s10052-019-6683-x. arXiv: 1901.07401 [astro-ph, physics:hep-ex, physics:physics].

[41] J. Aalbers et al. “First Dark Matter Search Results from the LUX-ZEPLIN (LZ) Experiment”. In: *Physical Review Letters* 131.4 (July 28, 2023), p. 041002. DOI: 10.1103/PhysRevLett.131.041002. arXiv: 2207.03764 [hep-ex].

[42] E. Aprile et al. “Search for Coherent Elastic Scattering of Solar ^{8}B Neutrinos in the XENON1T Dark Matter Experiment”. In: *Phys. Rev. Lett.* 126 (Mar. 1, 2021), p. 091301. DOI: 10.1103/PhysRevLett.126.091301. arXiv: 2012.02846 [hep-ex].

[43] Yue Meng et al. "Dark Matter Search Results from the PandaX-4T Commissioning Run". In: *Phys. Rev. Lett.* 127.26 (Dec. 23, 2021), p. 261802. DOI: 10.1103/PhysRevLett.127.261802. arXiv: 2107.13438 [hep-ex].

[44] P. Agnes et al. "Search for Dark-Matter–Nucleon Interactions via Migdal Effect with DarkSide-50". In: *Phys. Rev. Lett.* 130.10 (Mar. 6, 2023), p. 101001. DOI: 10.1103/PhysRevLett.130.101001. arXiv: 2207.11967 [hep-ex].

[45] A.H. Abdelhameed, G. Angloher, P. Bauer, et al. "First Results from the CRESST-III Low-Mass Dark Matter Program". In: *Physical Review D* 100.10 (Nov. 26, 2019), p. 102002. DOI: 10.1103/PhysRevD.100.102002. arXiv: 1904.00498 [astro-ph.CO].

[46] M. F. Albakry et al. "A Search for Low-mass Dark Matter via Bremsstrahlung Radiation and the Migdal Effect in SuperCDMS". In: *Physical Review D* 107.11 (June 1, 2023), p. 112013. DOI: 10.1103/PhysRevD.107.112013. arXiv: 2302.09115 [hep-ex].

[47] Christopher Savage et al. "Compatibility of DAMA/LIBRA Dark Matter Detection with Other Searches". In: *Journal of Cosmology and Astroparticle Physics* 04.04 (2009), p. 010. DOI: 10.1088/1475-7516/2009/04/010. arXiv: 0808.3607 [astro-ph].

[48] G. Adhikari et al. "Strong Constraints from COSINE-100 on the DAMA Dark Matter Results Using the Same Sodium Iodide Target". In: *Science Advances* 7.46 (Nov. 2021), abk2699. DOI: 10.1126/sciadv.abk2699. arXiv: 2104.03537 [hep-ex].

[49] C. Amole, M. Ardid, I.J. Arnquist, et al. "Dark Matter Search Results from the Complete Exposure of the PICO-60 ${\mathrm{C_{3}{\mathrm{F_{8}}$ Bubble Chamber". In: *Physical Review D* 100.2 (July 10, 2019), p. 022001. DOI: 10.1103/PhysRevD.100.022001. arXiv: 1902.04031 [astro-ph.CO].

[50] E. Behnke et al. "Final Results of the PICASSO Dark Matter Search Experiment". In: *Astroparticle Physics* 90 (Apr. 2017), pp. 85–92. DOI: 10.1016/j.astropartphys.2017.02.005. arXiv: 1611.01499 [hep-ex].

[51] D.S. Akerib, S. Alsum, H.M. Araújo, et al. "Limits on Spin-Dependent WIMP-nucleon Cross Section Obtained from the Complete LUX Exposure". In: *Physical Review Letters* 118.25 (June 23, 2017), p. 251302. DOI: 10.1103/PhysRevLett.118.251302. arXiv: 1705.03380 [astro-ph.CO].

[52] Andrew Gould. "Weakly Interacting Massive Particle Distribution in and Evaporation from the Sun". In: *The Astrophysical Journal* 321 (1987), p. 560. DOI: 10.1086/165652.

[53] Andrew Gould. "Resonant Enhancements in WIMP Capture by the Earth". In: *Astrophys. J.* 321 (1987), p. 571. DOI: 10.1086/165653.

[54] Giorgio Busoni et al. “Evaporation and Scattering of Momentum- and Velocity-Dependent Dark Matter in the Sun”. In: *Journal of Cosmology and Astroparticle Physics* 10.10 (Oct. 23, 2017), p. 037. DOI: 10.1088/1475-7516/2017/10/037. arXiv: 1703.07784 [hep-ph].

[55] W. H. Press and D. N. Spergel. “Capture by the Sun of a Galactic Population of Weakly Interacting, Massive Particles”. In: *The Astrophysical Journal* 296 (1985), pp. 679–684. DOI: 10.1086/163485.

[56] Chris Kouvaris. “WIMP Annihilation and Cooling of Neutron Stars”. In: *Physical Review D* 77.2 (2008), p. 023006. DOI: 10.1103/PhysRevD.77.023006. arXiv: 0708.2362 [astro-ph].